JACS
JOURNAL OF THE AMERICAN CHEMICAL SOCIETY
pubs.acs.org/JACS
Article

Ultrafine Rhodium–Chromium Mixed-Oxide Cocatalyst with Facet-Selective Loading for Excellent Photocatalytic Water Splitting

Daisuke Hirayama, Tokuhisa Kawawaki,* Sota Oguchi, Mai Ogano, Naochika Kon, Tomohiro Yasuda, Akihiro Higami, and Yuichi Negishi*

Cite This: https://doi.org/10.1021/jacs.4c07351
Read Online

ABSTRACT: The development of water-splitting photocatalysts capable of generating green hydrogen (H_2) from water and sunlight is crucial for achieving carbon neutrality. Further enhancement of the photocatalytic water-splitting activity is essential to realizing this objective. Photocatalysts with specific exposed crystal facets can facilitate efficient charge separation of electrons/holes, thereby achieving high activity for water splitting. However, there have been no reports of ultrafine (~1 nm) cocatalysts being loaded onto specific crystal facets of photocatalysts, despite cocatalysts being the actual reaction sites for water splitting. This study establishes a novel method for achieving facet-selective loading of ultrafine H_2-evolution cocatalysts onto the {100} facets, which are the H_2-evolution facets, of a strontium titanate photocatalyst. The resulting photocatalyst exhibits the highest apparent quantum yield achieved to date for strontium titanate. This research holds the potential to further improve various types of advanced photocatalysts and is expected to accelerate the transition to carbon neutrality.

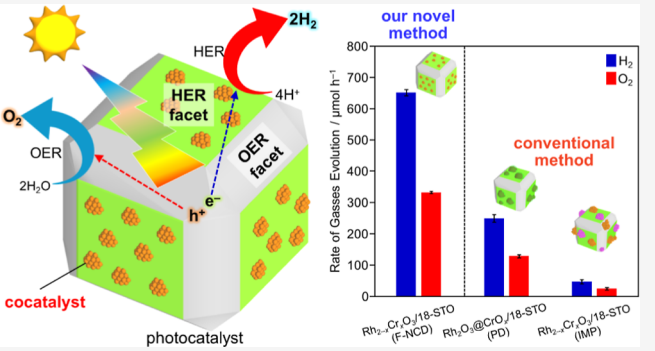

INTRODUCTION

One approach to achieving carbon neutrality is the transition to a hydrogen (H_2)-based energy society. Using water-splitting photocatalysts, green H_2 can be produced from only water and sunlight without emitting carbon dioxide (Figure 1a).[1−7] Water-splitting photocatalysts can produce H_2 more cheaply than water electrolysis because they do not require power generators, voltage control devices, and electrodes.[6] It is estimated that 5−10% of solar-to-H_2 conversion efficiency is required for practical application of water-splitting photocatalysts; improving the performance of water-splitting photocatalysts is currently being actively conducted.[2,7,8]

Water-splitting photocatalysts consist of a semiconductor photocatalyst that absorbs light and metal or metal oxide particles called cocatalysts (Figure 1). Cocatalysts act as the reaction site and play a crucial role in promoting reaction rates and charge separation (Figure 1a). Functionalizing cocatalysts can effectively improve the activity and durability of photocatalysts.[9−11] Generally, a cocatalyst is loaded onto a photocatalyst by conventional PD[12−14] (Figure 1d) or IMP[15−17] (Figure 1e) methods. Although these methods are technically straightforward, it is inherently challenging to precisely control the size and electronic structure of the cocatalyst. Loading a cocatalyst with finer particles results in much larger mass activity because of the increase of the specific surface area of the cocatalyst.[18−20] For this reason, a novel loading method has recently been established in which fine metal nanoclusters (NCs) with a particle size of about 1 nm are precisely synthesized in advance[21−24] and then loaded on photocatalysts (denoted as NCD; Figure 1c). There are many reports showing that the NCD method increased the water-splitting activity of photocatalysts.[9,25−29]

Some photocatalysts have a specific crystal facet to which excited electrons or holes easily transfer.[8,30,31] This is because the ease of electron or hole transfer depends on the difference of the work function on each crystal facet.[8] Selective loading of appropriate H_2-evolution[9,32−34] and oxygen (O_2)-evolution[30,31] cocatalysts on electron- and hole-transfer crystal facets, respectively, can improve the activity of water-splitting photocatalysts by promoting efficient space-charge separation and reaction.[8,30,31,35−38] Previous studies have revealed that the PD method can be used to selectively load H_2- and O_2-evolution cocatalysts on crystal facets, to which excited electrons and holes, respectively, can move easily.[31] In the NCD method, the cocatalyst is loaded nonselectively onto the

Received: May 30, 2024
Revised: September 7, 2024
Accepted: September 9, 2024

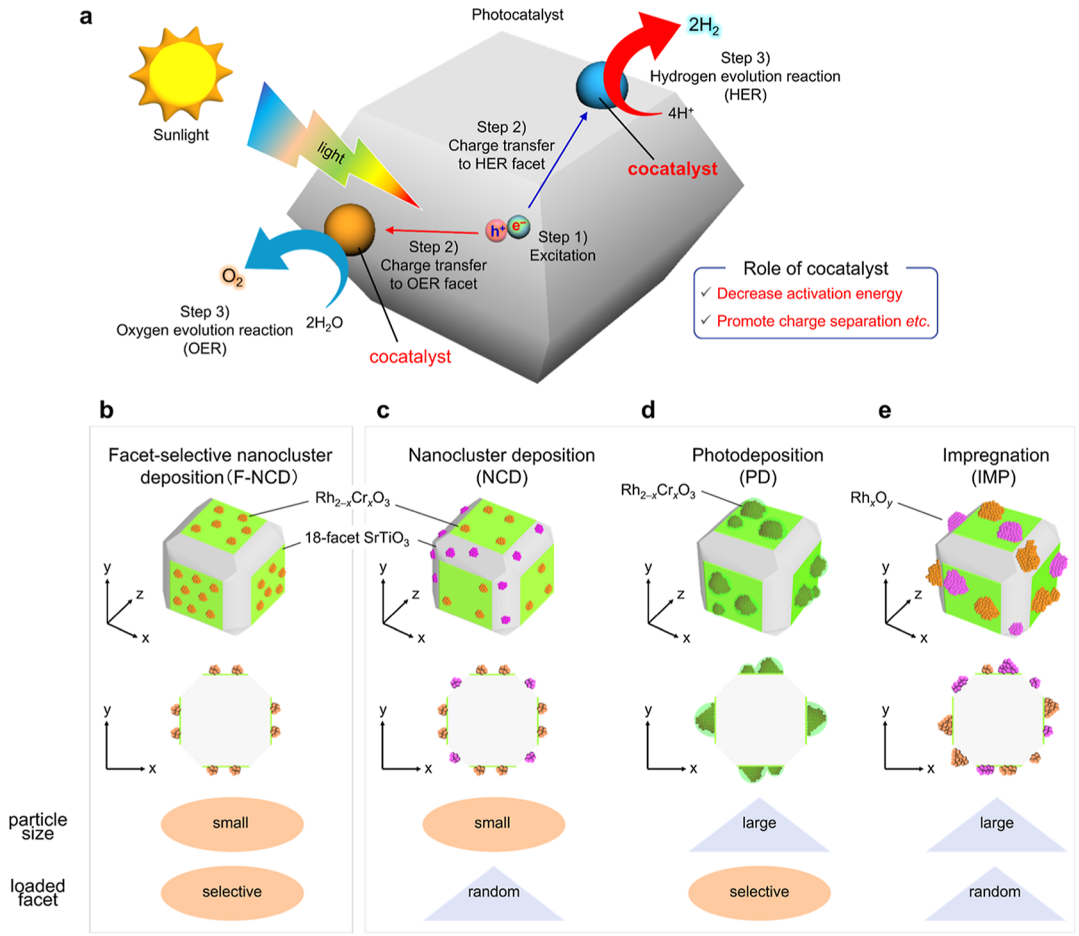

Figure 1. Background and purpose of this research. (a) Schematic illustration of water-splitting photocatalysis. Schematic diagrams of cocatalyst deposition methods on a photocatalyst for (b) facet-selective nanocluster deposition (F-NCD; this work) and conventional (c) nanocluster deposition (NCD), (d) photodeposition (PD), and (e) impregnation (IMP). IMP is an easy method to load cocatalysts, but it is difficult to control both particle size and loaded crystal facets. PD can be facet-selectively loaded cocatalysts, but it is difficult to control the particle size. NCD can control particle size of cocatalysts, but the particles are loaded on crystal facets randomly. In contrast, the F-NCD method makes it possible to facet-selectively load ultrafine cocatalysts while maintaining a fine particle size.

photocatalyst by forming chemical bonds between the ligands of the metal NCs and photocatalyst surface.[9,25] Consequently, NC cocatalysts are loaded even on crystal facets, where the desired reaction does not occur (Figure 1c). In this study, we establish F-NCD (Figure 1b), in which a fine H_2-evolution cocatalyst with a particle size of about 1 nm is selectively loaded onto the H_2-evolution facets of a photocatalyst. Specifically, we modify NCD by suppressing the chemical adsorption of cocatalyst precursors [rhodium (Rh) complexes] on the O_2-evolution facets by protecting these facets with organic compounds. We also enhance the selective adsorption of the Rh complexes on the H_2-evolution crystal facets using photoreductive adsorption (Figure 2). Using the F-NCD method, 1.2 nm $Rh_{2-x}Cr_xO_3$ (Rh−Cr) cocatalyst as a H_2-evolution cocatalyst is selectively loaded on the {100} facets (the H_2-evolution facets) of a strontium titanate ($SrTiO_3$; STO) photocatalyst (Figures 1b, 2a−e, and S1). The cocatalyst-loaded STO photocatalyst obtained by the F-NCD method exhibits an apparent quantum yield (AQY) 2.2 times higher than that of cocatalyst-loaded STO prepared by the conventional PD method. This AQY is the highest obtained to date for STO synthesized by hydrothermal synthesis. The F-NCD method is extended to other photocatalysts and NCs to demonstrate its versatility.

RESULTS AND DISCUSSION

Preparation and Characterization of Cocatalysts Using F-NCD on Photocatalysts. First, 18-STO, and 6-facets STO (6-STO) for comparison, was synthesized by hydrothermal synthesis according to previous reports (Figures 3a,b and S2).[30,39] In the PXRD pattern of 18-STO (Figure S2), peaks were observed at 68 and 47° that were consistent with the (220) and (200) reflections, respectively. This confirmed that both {110} and {100} facets are exposed in 18-STO. Excited electrons and holes tend to move to the {100} and {110} facets, which act as H_2- and O_2-evolution facets, respectively, in water-splitting reactions.[8]

The glutathione (SG)-protected Rh complexes (Rh−SG) as the precursor of the NC cocatalysts were prepared by our established method (Figure S3a).[9] Ultraviolet−visible spectroscopy confirmed that Rh−SG was similar to that obtained previously; therefore, it contained $Rh_2(SG)_2$ as the main compound (Figure S3b). TEM confirmed that the fine particle size of Rh−SG was 0.8 ± 0.1 nm (Figure 3c). We attempted to selectively load the obtained Rh−SG onto the {100} facets of 18-STO. Previous studies revealed that introducing chromium oxide (Cr_2O_3) on the H_2-evolution cocatalyst suppressed the reverse reaction on the cocatalyst surface as well as preventing cocatalyst aggregation,[40−42] thereby increasing photocatalytic

https://doi.org/10.1021/jacs.4c07351
J. Am. Chem. Soc. XXXX, XXX, XXX−XXX

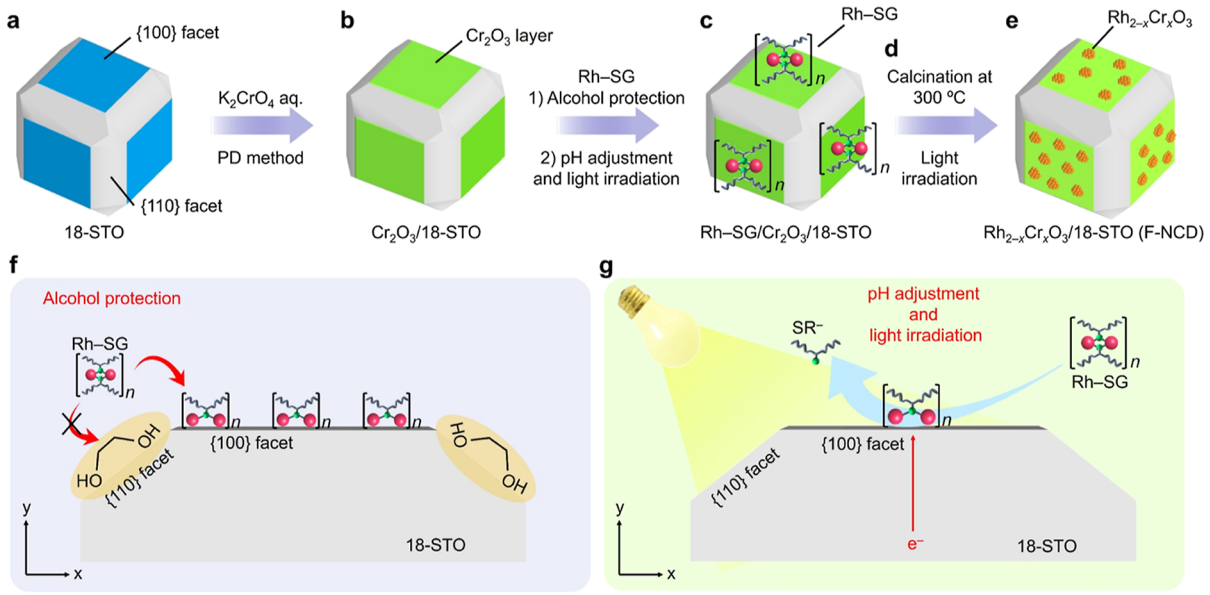

Figure 2. Schematic illustrations of F-NCD and strategies for facet-selective and efficient loading of ultrafine $Rh_{2-x}Cr_xO_3$ NC cocatalysts. (a–e) Steps for prepation methods of F-NCD. (f,g) Two strategies for facet-selective and efficient loading of ultrafine $Rh_{2-x}Cr_xO_3$ NC cocatalysts on the {100} facets (H_2-evolution facets) of 18-facet STO (18-STO).

activity and durability. Therefore, in this study, to finally load the solid-solution Rh–Cr cocatalyst on the {100} facets, a Cr_2O_3 layer was first loaded on the {100} facets of 18-STO (Cr_2O_3/18-STO) by PD (Figure 2b).[27] HAADF-STEM images and elemental mapping by EDS confirmed that the Cr_2O_3 layer of Cr_2O_3/18-STO was loaded only on the {100} facets of 18-STO (Figure S4a,b). During PD, Cr_2O_3 is loaded on facets to which excited electrons can easily move. It is interpreted that the Cr_2O_3 layer was selectively loaded on the {100} facets of 18-STO. Corresponding Cr K-edge XANES spectra (Figure S4c) showed that the rise of the white line observed at ∼6000 eV is in good agreement with that of the standard Cr_2O_3 sample and Cr_2O_3/18-STO, indicating that the loaded Cr_2O_3 layer had an electronic state consistent with that of Cr(III).

Next, we attempted to adsorb Rh–SG on the {100} facets of Cr_2O_3/18-STO (Figure 2c). If NC deposition is conducted without special treatment, Rh–SG adsorbs randomly on both {100} and {110} facets of 18-STO driven by hydrophilic interactions (such as OH···O and NH···O) between SG and STO or Cr_2O_3. To achieve the selective adsorption of Rh–SG on {100} facets of 18-STO, we suppressed Rh–SG adsorption on the {110} facets of 18-STO by appropriate compound protection (**strategy 1**; Figure 2f) and promoted Rh–SG adsorption on the {100} facets of 18-STO through photo-induced ligand desorption from Rh–SG (**strategy 2**; Figure 2g).

Regarding **strategy 1**, certain organic compounds adsorb only on specific crystal facets of semiconductors driven by the different surface charges of crystal facets.[43] Using this property, we attempted to protect the {110} facets of 18-STO with an appropriate organic compound prior to Rh–SG adsorption. This would suppress the adsorption of Rh–SG on the {110} facets, leading to the facet-selective adsorption of Rh–SG on the {100} facets. Therefore, we searched for an appropriate organic compound that adsorbed selectively on the {110} facets of 18-STO (Figures S5 and S6a). The results revealed that EG adsorbed on 18-STO with {110} facets but did not adsorb on 6-STO with only {100} facets from the results of FT-IR spectra (Figure 3f). Accordingly, we used EG as an organic additive to protect the {110} facets of 18-STO and enable selective adsorption of Rh–SG on the {100} facets of 18-STO.[43] Further experiments showed that an appropriate amount of EG was needed to be added to achieve facet-selective loading (Figure S6b).

However, when using only **strategy 1**, Rh–SG was adsorbed on 18-STO with an adsorption rate of only 49%. Therefore, we also developed **strategy 2** to increase the adsorption rate of Rh–SG on 18-STO. The amount of Rh–SG adsorbed on the {100} facets of Cr_2O_3/18-STO is dominated by the adsorption equilibrium at the interface between Cr_2O_3/18-STO and water. Therefore, if the ligand of Rh–SG is removed by photoexcited electrons, the ligand-removed Rh–SG forms strong bonds with Cr_2O_3/18-STO and thereby, Rh–SG is expected to readily adsorb on Cr_2O_3/18-STO. It is expected that when Rh–SG/Cr_2O_3/18-STO is photoirradiated under basic conditions, thiolate (SR) could be desorbed from Rh–SG using excited electrons generated by photoirradiation of Cr_2O_3/18-STO ($M_n(SR)_m + e^- \rightarrow M_n(SR)_{m-1} + SR^-$)[44] (Figure 2g). Because the exposed Rh site generated by this reaction forms a Rh–O bond with Cr_2O_3, Rh–SG is unlikely to redissolve in water. Based on these predictions, Rh–SG adsorption was conducted under photoirradiation, unlike in our previous studies.[9] Also, Rh–SG is unstable under strongly basic conditions (Figure S7), and photoirradiation was performed under relatively mild basic conditions (pH = 10), where Rh–SG can exist stably. Using **strategy 2**, the adsorption rate of Rh–SG was successfully increased to ∼95%. Figure 3i–k shows HAADF-STEM images of the obtained photocatalyst (Rh–SG/Cr_2O_3/18-STO). Almost no particles were observed on the {110} facets (Figure 3k), whereas amorphous particles were observed on the {100} facets (Figure 3j). The results of EDS elemental mapping confirmed the presence of Rh in the amorphous particles (Figure 3l–p). A Rh K-edge FT-EXAFS spectra (Figure 3d) confirmed that Rh–SG after adsorption formed Rh–O bonds

https://doi.org/10.1021/jacs.4c07351
J. Am. Chem. Soc. XXXX, XXX, XXX–XXX

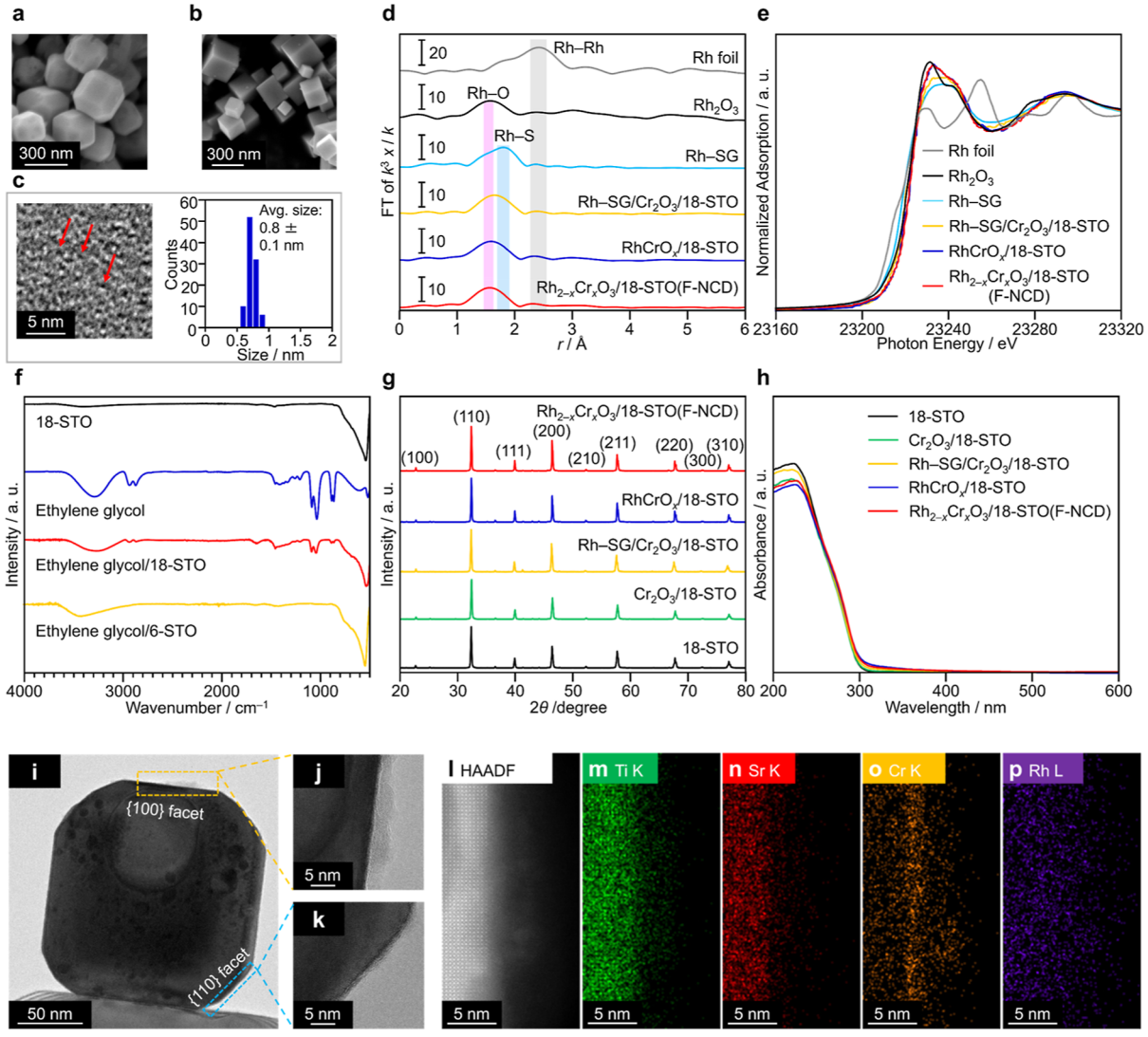

Figure 3. Characterization of the 18-STO photocatalyst and Rh−Cr cocatalyst. Scanning electron microscopy (SEM) images of (a) 18-STO and (b) 6-STO. (c) Transmission electron microscopy (TEM) image and size histogram of Rh−SG. (d) Rh K-edge Fourier-transform extended X-ray absorption fine structure (FT-EXAFS) spectra and (e) Rh K-edge X-ray absorption near-edge structure (XANES) spectra of the 18-STO after each step of F-NCD. (f) FTinfrared (FT-IR) spectra of 6- and 18-STO after adsorption of ethylene glycol (EG). (g) Powder X-ray diffraction (PXRD) patterns and (h) diffuse-reflectance (DR) spectra of the 18-STO after each step of F-NCD. (i−k) TEM and (l) high-angle annular dark-field scanning TEM (HAADF-STEM) images and (m−p) energy-dispersive X-ray spectroscopy (EDS) elemental mapping (Ti−K, Sr−K, Cr−K, and Rh−L) of $Rh_{2-x}Cr_xO_3$/18-STO prepared by F-NCD. In (d,e), the spectra of Rh foil and Rh_2O_3 and the standards for Rh(0) and Rh(III) are also shown, respectively. In (f), the FT-IR spectrum of EG is also shown for comparison. Images in (j) and (l−p) were focused on the {100} facets of 18-STO. The image in (k) was focused on the {110} facets of 18-STO.

(~1.6 Å) in addition to Rh−S bonds (~1.9 Å). Rh K-edge XANES spectra (Figure 3e) showed that the rising white line at ~23,200 eV of Rh−SG after adsorption is shifted to higher energy than that of Rh−SG before adsorption, indicating that it is slightly oxidized based on the desorption of electron-donating SG. These results indicate that conducting **strategy 1** and **2** enabled selective and efficient Rh−SG adsorption on the {100} facets of Cr_2O_3/18-STO.

The presence of organic compounds on photocatalysts hinders reactant approach and electron transfer from the photocatalyst to the cocatalyst, which often suppresses photocatalytic activity.[9,19,20] Therefore, most of the remaining ligands (SG and EG) were removed by calcination of Rh−SG/Cr_2O_3/18-STO at 300 °C (Figure 2d).[9,11,27,45] Figure 3d,e,g,h shows the characterization results for the photocatalyst after calcination at 300 °C ($RhCrO_x$/18-STO). In the Rh K-edge FT-EXAFS spectrum after calcination, the peak intensity of Rh−S bonds was relatively weak, and a more distinct peak of Rh−O bonds was observed (Figure 3d). This indicates ligand desorption and further immobilization to 18-STO based on Rh−S bond dissociation of Rh−SG. These characterization results indicated that calcination at 300 °C resulted in the desorption of remaining ligands while keeping the structure of 18-STO (Figures 3g,h and S8).

In $RhCrO_x$/18-STO, some Cr ions were highly oxidized [>Cr(III)] (Figure S4c).[9] We reduced it to Cr^{3+} by photoirradiation of the photocatalyst in water [Figure 2e; $Rh_{2-x}Cr_xO_3$/18-STO(F-NCD)]. HAADF-STEM images and EDS elemental mapping (Figure 3i−p) confirmed that Rh and Cr were in the same layer on the {100} facets in $Rh_{2-x}Cr_xO_3$/18-STO(F-NCD). This indicates that the Rh−Cr cocatalyst, which consisted of a solid solution of Rh(III) and Cr(III)

https://doi.org/10.1021/jacs.4c07351
J. Am. Chem. Soc. XXXX, XXX, XXX−XXX

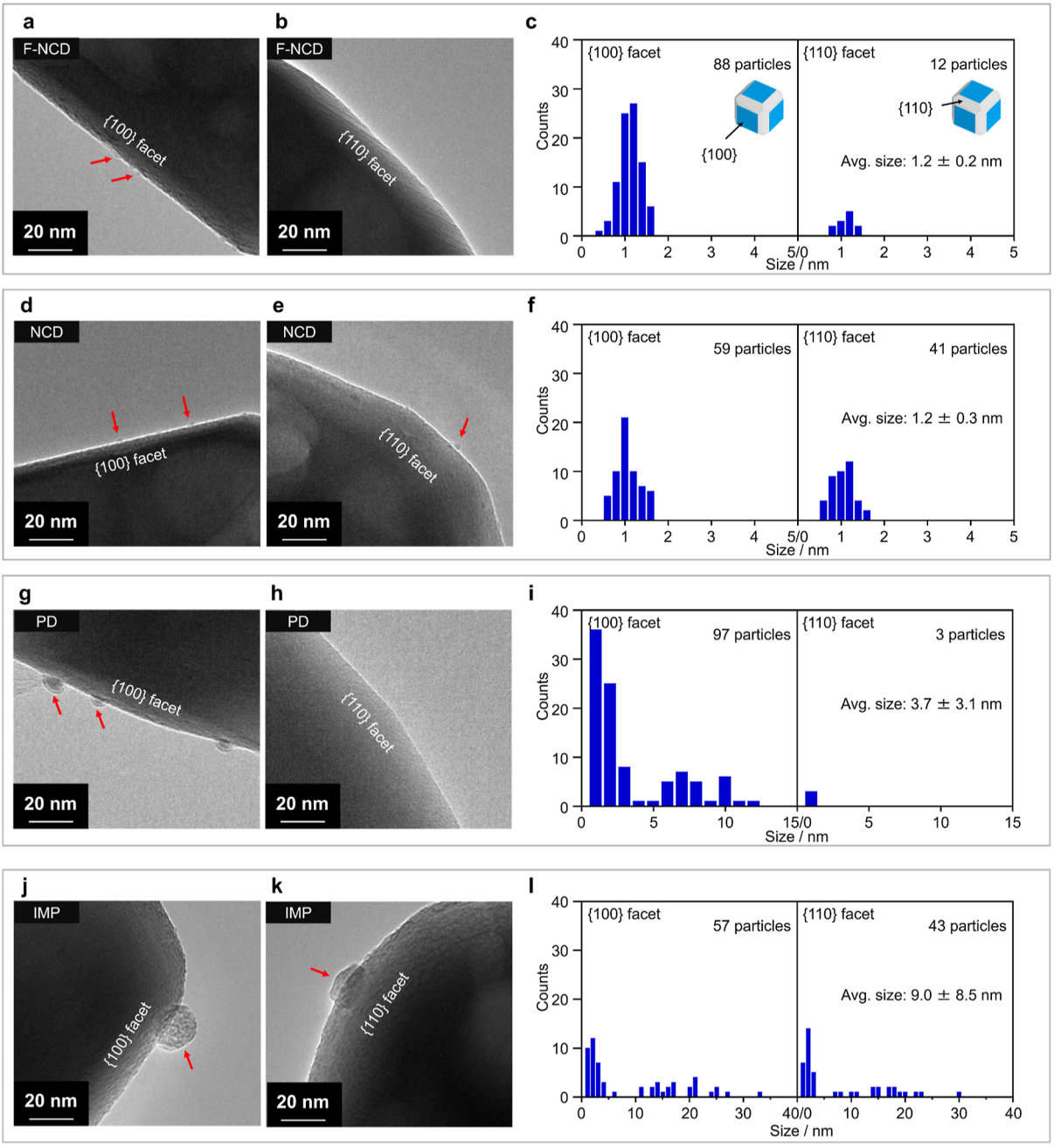

Figure 4. Characterization of the Rh−Cr cocatalyst prepared by F-NCD, NCD, PD, and IMP. TEM images of the cocatalyst prepared by (a,b) F-NCD, (d,e) NCD, (g,h) PD, and (j,k) IMP on the (a,d,g,j) {100} and (b,e,h,k) {110} facets of Cr-loaded 18-STO. Histograms of the particle size and the loading ratio on the {100} and {110} facets of 18-STO of the-cocatalysts loaded on Cr-coated 18-STO prepared by (c) F-NCD, (f) NCD, (i) PD, and (l) IMP. 18-STO (~20 particles) prepared in each method was randomly selected to calculate the crystal facets and size of the loaded cocatalyst.

oxides, was loaded on the {100} facets of 18-STO (Table S1 and Figures 3e and S4c).[9] The XPS (Figure S9) and FT-IR spectra (Figure S10) of $Rh_{2-x}Cr_xO_3$/18-STO(F-NCD) revealed that photoirradiation resulted in the complete removal of the ligands that remained on photocatalysts after calcination.[46] The PXRD patterns (Figure 3g), DR spectra (Figure 3h), and FT-IR spectra (Figure S10) of $Rh_{2-x}Cr_xO_3$/18-STO(F-NCD) confirmed that photoirradiation did not affect the 18-STO.

As described below, TEM measurements revealed that the particle size of the loaded $Rh_{2-x}Cr_xO_3$ NC cocatalysts was 1.2 ± 0.2 nm, and the selective loading ratio on the {100} facets (the number of NC cocatalysts on the {100} facets/total number of NC cocatalysts) was 88% (Figure 4a−c). These results indicate that we loaded ultrafine 1.2 nm $Rh_{2-x}Cr_xO_3$ NC cocatalysts on the H_2-evolution facets of 18-STO with high selectivity and adsorption efficiency by applying two additional strategies to the previously reported NCD method.[9] Further studies revealed that a calcination temperature of 300 °C is important to obtain highly active photocatalysts by F-NCD (Figure S11).

Comparison of Rh−Cr Cocatalyst-Modified 18-STO Photocatalysts Prepared by Different Methods. The particle size, location, and electronic state of the NC

https://doi.org/10.1021/jacs.4c07351
J. Am. Chem. Soc. XXXX, XXX, XXX−XXX

cocatalysts in the obtained $Rh_{2-x}Cr_xO_3$/18-STO(F-NCD) were compared with those in photocatalysts prepared by conventional methods (Figures 4 and S12−S18). Cocatalyst-loaded photocatalysts prepared by PD[41] [$Rh_{2-x}Cr_xO_3$/18-STO(PD)], IMP [$Rh_{2-x}Cr_xO_3$/18-STO(IMP)], and our previously established NCD method[9] [$Rh_{2-x}Cr_xO_3$/18-STO-(NCD)], in which fine $Rh_{2-x}Cr_xO_3$ cocatalysts are randomly loaded on 18-STO facets, were used for comparison with $Rh_{2-x}Cr_xO_3$/18-STO(F-NCD). 18-STO (∼20 particles) prepared in each method was randomly selected for TEM analysis. The average particle size and loading facets ({100} or {110} facets) of the loaded cocatalysts were estimated from TEM measurements (Figures S12−S16). A representative TEM image and a size histogram of the cocatalysts loaded on each crystal facet are summarized in Figures 4 and S12. The electronic structure and coordination structure of the loaded cocatalysts were estimated from Rh K-edge XAFS (Figure S17) and Cr K-edge XANES spectra (Figure S18).

Regarding the particle size of the cocatalysts, as discussed earlier, the diameter of NC-cocatalysts prepared by F-NCD was 1.2 ± 0.2 nm (Figures 4a−c and S13). The NCD method is similar to F-NCD except that it lacks additional strategies for selective facet deposition. Therefore, the same cocatalyst particle size (1.2 ± 0.3 nm) was obtained using the NCD method as that from the F-NCD method (Figures 4d−f and S14). The SG ligand inhibits the aggregation of Rh−SGs on the 18-STO surface, which likely allows both F-NCD and NCD methods to load NC cocatalysts while maintaining its fine size. In contrast, the particle sizes of cocatalysts loaded by PD (Figures 4g−i and S15) and IMP (Figures 4j−l and S16) methods were 3.7 ± 3.1 and 9.0 ± 8.5 nm, respectively. This means that the NC cocatalysts loaded by F-NCD were only 32 and 13% smaller than those loaded by PD and IMP, respectively. The particle size distribution of NC cocatalysts loaded by F-NCD was also much narrower than those of the cocatalysts loaded by PD and IMP methods (Figures 4c,i,l and S12).

Regarding the location of the cocatalysts, the selective loading ratio on the {100} facets was 57 and 59% for IMP (Figure 4l) and NCD (Figure 4f) methods, respectively. The slightly higher selectivity for {100} facets over {110} facets was ascribed to the different surface areas of {100} and {110} facets in 18-STO (1.83×10^4 and 1.25×10^4 nm,[2] respectively). These results indicate that IMP and NCD methods load cocatalyst nonselectively on the crystalline facets. Conversely, F-NCD (Figure 4c) and PD (Figure S4i) methods loaded cocatalysts on the {100} facets of 18-STO with high selectivities of 88 and 97%, respectively. During the PD method, the Rh-based cocatalyst can be selectively loaded on the facets where excited electrons reach (i.e., the {100} facets of 18-STO),[31] because only Rh ions adsorbed on the {100} facets are photoreduced. In the case of the F-NCD method, facet selectivity was improved by **strategy 1** and **2** described above. The present results demonstrate that the F-NCD method can also load NC cocatalysts on target crystal facets with high selective loading rates close to those achieved by the PD method.

Both Rh K-edge XANES (Figure S17a) and Cr K-edge XANES spectra (Figure S18) showed that the electronic structures of Rh and Cr in the cocatalysts loaded by different methods were almost similar. The loaded cocatalysts had stable oxidation states (Rh^{3+} and Cr^{3+}), indicating that the loading method did not strongly affect the electronic states of the cocatalysts. Furthermore, Rh K-edge EXAFS measurements indicated the absence of Rh−Rh or Rh−S bonds in the cocatalysts prepared by all methods (Figure S17b,c). This suggests that the coordination structure of the Rh is similar and is predominantly based on Rh−O bonds (Table S1).

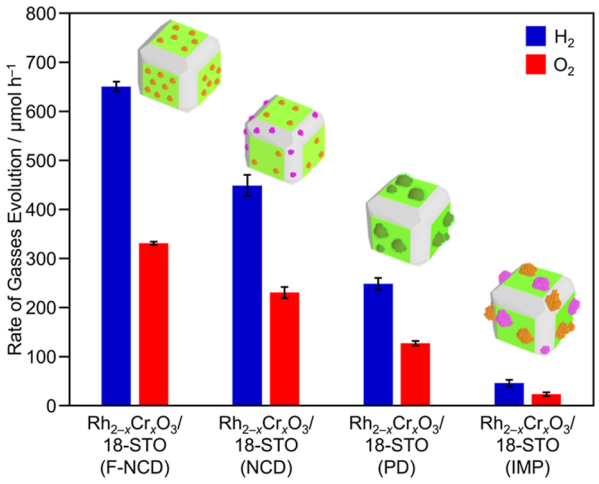

Figure 5. Comparison of the overall water-splitting activity of photocatalysts. Comparison of the activities of Rh−Cr cocatalyst-loaded 18-STO prepared by F-NCD, NCD, PD, and IMP. Loading weights of Rh and Cr were 0.1 and 0.2 wt %, respectively.

Performance of Photocatalysts in Overall Water Splitting. The photocatalytic water-splitting activity of $Rh_{2-x}Cr_xO_3$/18-STO(F-NCD) with different loading amounts of Cr and Rh was measured. The highest activity was obtained when the loading weights of Cr and Rh were 0.2 and 0.1 wt %, respectively (Figure S19). The photocatalyst prepared by the optimized F-NCD method showed water-splitting activity that was 2.6 and 14 times higher than that of photocatalysts prepared by PD and IMP methods, respectively (Figure 5). Here, even with shorter light irradiation times and fewer cocatalyst precursors in the conventional PD method to make finer cocatalysts, higher activity could not be achieved compared with the F-NCD method (Figure S20). In addition, the water-splitting activity of $Rh_{2-x}Cr_xO_3$/18-STO(F-NCD) was 1.5 times higher than that of the photocatalyst prepared by the conventional NCD method (Figure 5).

To clarify the origin of the high activity of the photocatalyst prepared by F-NCD, we investigated the applied-voltage dependence of the photoresponse of photocatalysts by using photoelectrodes (Figure 6a). The negative current arising from H_2 evolution increased with the applied negative potential, and this current further increased under photoirradiation. This indicates that H_2 evolution occurred by electrons generated by photoexcitation to the conduction band of 18-STO. Additionally, the order of photocurrent density was consistent with that of photocatalytic water-splitting activity [$Rh_{2-x}Cr_xO_3$/18-STO(F-NCD) > $Rh_{2-x}Cr_xO_3$/18-STO(NCD) > $Rh_{2-x}Cr_xO_3$/18-STO(PD) > $Rh_{2-x}Cr_xO_3$/18-STO(IMP); Figure 6a]. Impedance measurements confirmed that the cocatalyst loading did not affect the conductivity of 18-STO (Figure 6b). The fact that a low loading (0.1 wt %) of a fine cocatalyst (size: 1.2 nm) on a large size of 18-STO (size: ∼200 nm) does not affect its conductivity is a convincing result.[47] These results indicate that in $Rh_{2-x}Cr_xO_3$/18-STO(F-NCD), water reduction is promoted on the surface of the cocatalyst because of the fine particle size with a large specific surface area

https://doi.org/10.1021/jacs.4c07351
J. Am. Chem. Soc. XXXX, XXX, XXX−XXX

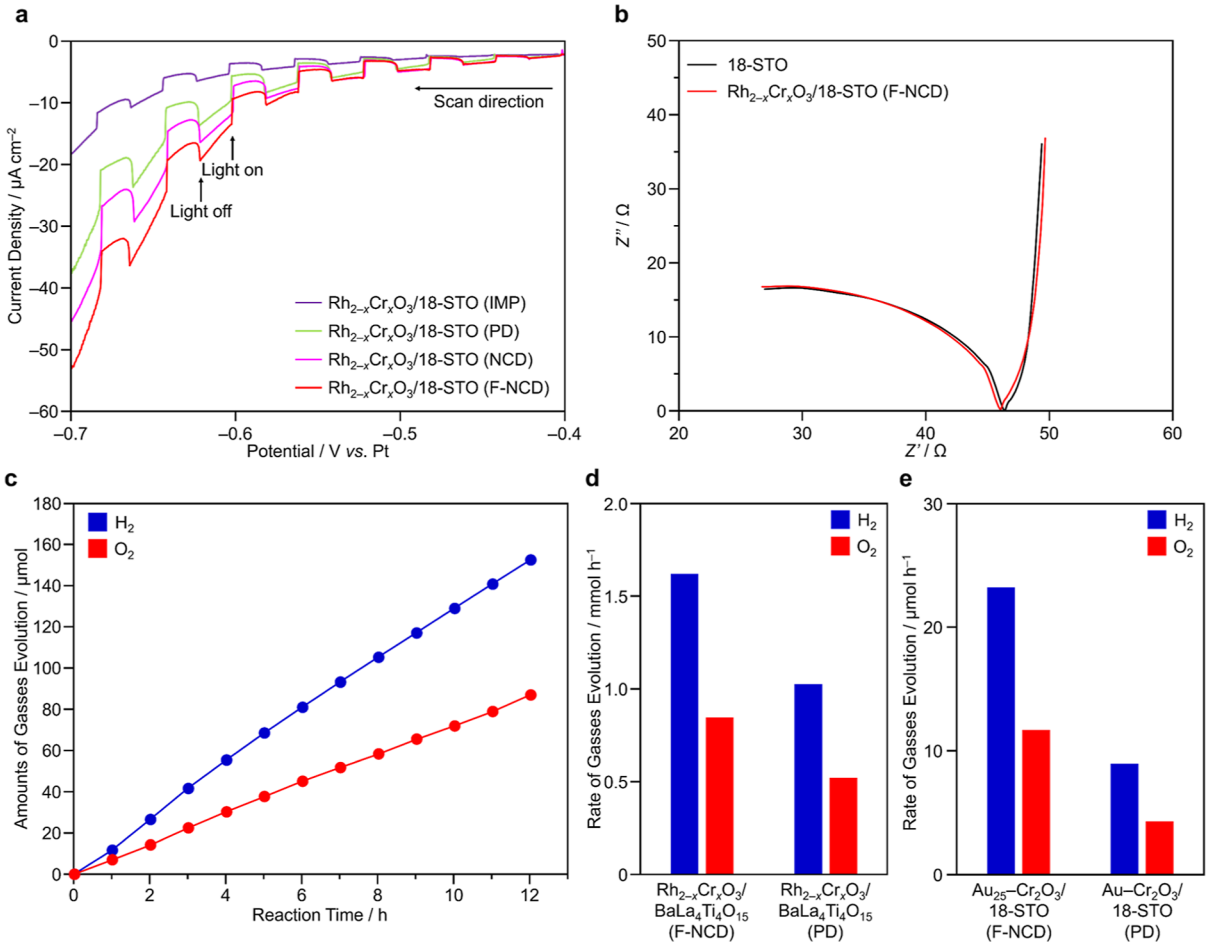

Figure 6. Photocatalytic properties of different photocatalysts. (a) Photocurrent responses of Rh−Cr cocatalyst-loaded 18-STO fabricated by different methods and (b) electrochemical impedance spectra of 18-STO and $Rh_{2-x}Cr_xO_3$/18-STO(F-NCD). (c) Time dependence of the water-splitting activity of $Rh_{2-x}Cr_xO_3$/18-STO(F-NCD). (d,e) Overall water-splitting activities of photocatalysts with Rh−Cr or Au−Cr cocatalysts prepared by F-NCD and PD.

and their facet-selective loading, leading to particularly high water-splitting activity.

The importance of facet-selective loading of cocatalysts was confirmed by comparing the water-splitting activities of the photocatalysts prepared by the F-NCD and NCD methods. In both photocatalysts, the amount of material loaded, particle size, and dispersity of the cocatalyst are almost the same. However, the selective loading ratio of NC-cocatalysts on the {100} facets in the photocatalyst prepared by the F-NCD method (88%) is approximately 1.5 times higher than that of the photocatalyst prepared by the NCD method (59%). This ratio is in good agreement with the activity ratio of the former to the latter, which is also 1.5, indicating a roughly linear proportional relationship between the crystal face selectivity and activity of the cocatalyst (Figure 5). As previously discussed, the water-splitting activity of the F-NCD method was 2.6 times higher than that of the PD method. Although the PD method exhibits slightly higher crystal facet selectivity compared to the F-NCD method (97% vs 88%), applying the activity enhancement effect of these crystal facet selectivities to the previously described linear proportional relationship, the activity enhancement due to the miniaturization of the cocatalyst is estimated to be about 2.9 times. This suggests that the impact of miniaturization (2.9-fold increase) plays a more significant role in enhancing activity than the effect of crystal facet selectivity (1.5-fold increase). From these findings, it was confirmed that facet-selective loading of ultrafine cocatalysts is important for achieving high water-splitting activity and the F-NCD method is an effective approach.

We estimated that the AQY of photocatalytic water splitting for $Rh_{2-x}Cr_xO_3$/18-STO(F-NCD) was 2.14% at 350 nm, which is the highest reported to date of STO synthesized by hydrothermal synthesis (Table S2). Additionally, after 12 h of photoirradiation, H_2 and O_2 were still generated at stoichiometric ratios, and the generation rate was approximately maintained (Figure 6c). No aggregation of the $Rh_{2-x}Cr_xO_3$ cocatalyst was observed after 12 h of photoirradiation, with the particle size maintained at 1.2 ± 0.3 nm, and no change of PXRD pattern based on 18-STO (Figure S21). However, a slight decrease in activity was observed, attributed to Cr elution, as detected by ICP-MS measurements (Figure S22). Furthermore, considering practical applications, we attempted a longer-term durability test. Measurements were carried out for 8 days, assuming approximately 8 h of sunlight exposure per day. As a result, the decrease in activity slowed after approximately 4 days of the activity test because the Cr elution reached a steady state (Figure S23).

Additionally, the results indicated that the codeposition of cobalt oxide (CoO_x) as an oxygen evolution reaction (OER) catalyst to $Rh_{2-x}Cr_xO_3$/18-STO(F-NCD) exhibited higher

https://doi.org/10.1021/jacs.4c07351
J. Am. Chem. Soc. XXXX, XXX, XXX−XXX

activity compared to when both HER and OER cocatalysts were codeposited using the PD method (Figure S24). Overall, the F-NCD method provided a photocatalyst with both high activity and high stability.

Versatility of F-NCD. We also investigated the applicability of F-NCD to another photocatalyst with specific exposed crystalline facets, $BaLa_4Ti_4O_{15}$,[48] which exhibits a high water-splitting activity. The results showed that the Rh−Cr cocatalyst-loaded $BaLa_4Ti_4O_{15}$ prepared by the F-NCD method [$Rh_{2-x}Cr_xO_3/BaLa_4Ti_4O_{15}$(F-NCD)] exhibited water-splitting activity that was 1.6 times higher than that of Rh−Cr cocatalyst-loaded $BaLa_4Ti_4O_{15}$ prepared by the PD method [$Rh_{2-x}Cr_xO_3/BaLa_4Ti_4O_{15}$(PD)] and 1.2 times higher than that of Rh−Cr cocatalyst-loaded $BaLa_4Ti_4O_{15}$ prepared by NCD [$Rh_{2-x}Cr_xO_3/BaLa_4Ti_4O_{15}$(NCD)][9] (Figures 6d and S25a). We also used NCs composed of other metals as cocatalyst precursors. When SG-protected Au_{25} clusters [$Au_{25}(SG)_{18}$; Au = gold; Figure S26] were used as cocatalyst precursors, the photocatalyst prepared by the F-NCD method [Au_{25}−Cr_2O_3/18-STO(F-NCD)] exhibited higher water-splitting activity than that of the corresponding photocatalyst prepared by the PD and NCD method [Au−Cr_2O_3/18-STO(PD) and Au_{25}−Cr_2O_3/18-STO(NCD)] (Figures 6e and S25b). These results demonstrate that F-NCD is an effective approach to enhance the activity of various advanced photocatalysts.

CONCLUSIONS

The activity of water-splitting photocatalysts can be substantially increased by using ultrafine NC cocatalysts with a particle size of ∼1 nm. However, a facet-selective loading method for such fine cocatalyst particles on photocatalysts has not been established. In this study, we synthesized fine Rh−SG complexes as a cocatalyst precursor. Then, we selectively loaded 1.2 nm $Rh_{2-x}Cr_xO_3$ NC cocatalysts on the H_2-evolution facets of 18-STO using two strategies: (1) suppressing Rh−SG adsorption on the O_2-evolution facets by protecting these facets with EG and (2) promoting Rh−SG adsorption on the H_2-evolution facets via photoinduced ligand desorption. The photocatalyst obtained using this developed F-NCD method achieved the highest AQY to date for a STO prepared by hydrothermal synthesis. We also confirmed that the F-NCD method can be applied to various photocatalysts and NCs. Doping STO with different metals can further enhance its activity[8] and make it responsive to visible light.[49] We expect that numerous water-splitting photocatalysts with high solar-to-H_2 conversion efficiency can be developed by combining advanced photocatalysts[50,51] with the F-NCD method and contribute to achieving carbon neutrality. In addition to these studies, it is necessary to develop more effective and durable materials for preventing the reverse reaction.

EXPERIMENTAL SECTION

Preparation of $Rh_{2-x}Cr_xO_3$/18-STO(F-NCD). First, 18-STO (250 mg) and ultrapure water (350 mL) were added to an internally irradiated reaction vessel to which an appropriate amount of K_2CrO_4 solution was added. After being degassed for 1 h under an argon gas flow at 30 mL min^{-1}, the suspension was irradiated with a 400 W mercury lamp for 1.5 h at 15 °C. The Cr_2O_3/18-STO powder was obtained by centrifugation. Cr_2O_3/18-STO (200 mg) and ultrapure water (120 mL) were added to a Pyrex glass irradiation cell and dispersed by sonication. EG (1.0 g) was added, and then the pH of the suspension was adjusted to 10 using sodium hydroxide. After the appropriate aqueous Rh−SG solution was added with stirring, the sample was irradiated with a 300 W xenon lamp (λ > 200 nm) for 45 min. The Rh−SG/Cr_2O_3/18-STO powder was collected by centrifugation and dried. Rh−SG/Cr_2O_3/18-STO was calcined at 300 °C under reduced pressure (∼2.0 × 10^{-1} Pa) and then photoirradiated using a 400 W mercury lamp to give $Rh_{2-x}Cr_xO_3$/18-STO(F-NCD) (Figure S2).

ASSOCIATED CONTENT

Supporting Information

The Supporting Information is available free of charge at https://pubs.acs.org/doi/10.1021/jacs.4c07351.

Experimental section; characterization; protocol used for the preparation of $Rh_{2-x}Cr_xO_3$/18-STO(F-NCD); PXRD patterns; synthesis method of Rh−SG; characterization of the Cr layer; FT-IR spectra; comparison of the activity of photocatalytic overall water splitting; stability test of Rh−SG; effect of the calcination at 300 °C for water splitting activity of 18-STO; results of sulfur 2p XPS spectra;th FT-IR spectra of Rh-cocatalyst-loaded 18-STO with the Cr layer; comparison of the calcination temperature of Rh cocatalyst-loaded 18-STO with the Cr layer; characterization of the $Rh_{2-x}Cr_xO_3$ cocatalyst; characterization of the $Rh_{2-x}Cr_xO_3$ cocatalyst prepared by F-NCD, NCD, PD, and IMP methods; comparison of the electronic state of the Rh cocatalyst; comparison of electronic state of Cr layer; comparison of Cr- and Rh-loading weight and light irradiation time for water-splitting activity; comparison of Rh-loading weight and light irradiation time; characterization of 18-STO and $Rh_{2-x}Cr_xO_3$ cocatalyst prepared by the F-NCD method; time course of water-splitting activity; time course of water-splitting activity for $Rh_{2-x}Cr_xO_3$/18-STO(F-NCD); comparison of the overall water-splitting activity of photocatalysts; comparison of water-splitting activity using other photocatalysts or metal NCs; characterization and stability test of $Au_{25}(SG)_{18}$; curve fitting analysis of Rh K-edge EXAFS data; and AQY of reported photocatalysts (PDF)

AUTHOR INFORMATION

Corresponding Authors

Tokuhisa Kawawaki − *Department of Applied Chemistry, Faculty of Science, Tokyo University of Science, Shinjuku-ku, Tokyo 162-8601, Japan; Carbon Value Research Center, Research Institute for Science and Technology, Tokyo University of Science, Noda, Chiba 278-8510, Japan;* orcid.org/0000-0003-3282-8964; Email: kawawaki@rs.tus.ac.jp

Yuichi Negishi − *Department of Applied Chemistry, Faculty of Science, Tokyo University of Science, Shinjuku-ku, Tokyo 162-8601, Japan; Carbon Value Research Center, Research Institute for Science and Technology, Tokyo University of Science, Noda, Chiba 278-8510, Japan; Institute of Multidisciplinary Research for Advanced Materials, Tohoku University, Sendai 980-8577, Japan;* orcid.org/0000-0003-3965-1399; Email: yuichi.negishi.a8@tohoku.ac.jp

Authors

Daisuke Hirayama − *Department of Applied Chemistry, Faculty of Science, Tokyo University of Science, Shinjuku-ku, Tokyo 162-8601, Japan*

https://doi.org/10.1021/jacs.4c07351
J. Am. Chem. Soc. XXXX, XXX, XXX−XXX

Sota Oguchi − *Department of Applied Chemistry, Faculty of Science, Tokyo University of Science, Shinjuku-ku, Tokyo 162-8601, Japan*
Mai Ogano − *Department of Applied Chemistry, Faculty of Science, Tokyo University of Science, Shinjuku-ku, Tokyo 162-8601, Japan*
Naochika Kon − *Innovation Center, Mitsubishi Materials Corporation, Naka-shi, Ibaraki 311-0102, Japan*
Tomohiro Yasuda − *Innovation Center, Mitsubishi Materials Corporation, Naka-shi, Ibaraki 311-0102, Japan*
Akihiro Higami − *Innovation Center, Mitsubishi Materials Corporation, Naka-shi, Ibaraki 311-0102, Japan*

Complete contact information is available at: https://pubs.acs.org/10.1021/jacs.4c07351

Funding

This work was supported by the Japan Society for the Promotion of Science (JSPS) KAKENHI (grant no. 24K01459, 23H00289, and 22K19012) and Scientific Research on Innovative Areas "Hydrogenomics" (grant no. 21H00027). Funding from the Yazaki Memorial Foundation for Science and Technology, Kao Foundation for Arts and Sciences, Sasakawa Scientific Research Grant from the Japan Science Society, and TEPCO Memorial Foundation Research Grant (Basic Research) is gratefully acknowledged.

Notes

The authors declare no competing financial interest.
Correspondence and requests for materials should be addressed to T.K. and Y.N.

■ ABBREVIATIONS

H_2	hydrogen
PD	photodeposition
IMP	impregnation
NCs	nanoclusters
NCD	nanocluster deposition
O_2	oxygen
F-NCD	facet-selective nanocluster deposition
Rh	rhodium
Rh−Cr	$Rh_{2-x}Cr_xO_3$
AQY	apparent quantum yield
STO	strontium titanate
18-STO	18-facets STO
6-STO	6-facets STO
PXRD	powder X-ray diffraction
SG	glutathione
Rh−SG	SG-protected Rh complexes
UV−vis	ultraviolet−visible
TEM	transmission electron microscopy
Cr_2O_3	chromium oxide
Cr_2O_3/18-STO	Cr_2O_3 layer was loaded on the {100} facets of 18-STO
HAADF-STEM	high-angle annular dark-field scanning TEM
EDS	energy-dispersive X-ray spectroscopy
XANES	X-ray absorption near-edge structure
EG	ethylene glycol
FT-IR	Fourier-transform infrared
SR	thiolate
Rh−SG/Cr_2O_3/18-STO	Rh−SG adsorbed on Cr_2O_3/18-STO
EXAFS	extended X-ray absorption fine structure
$RhCrO_x$/18-STO	Rh−SG/Cr_2O_3/18-STO calcined at 300 °C
$Rh_{2-x}Cr_xO_3$/18-STO(F-NCD)	cocatalyst-loaded photocatalysts prepared by F-NCD
$Rh_{2-x}Cr_xO_3$/18-STO(PD)	cocatalyst-loaded photocatalysts prepared by PD
$Rh_{2-x}Cr_xO_3$/18-STO(IMP)	cocatalyst-loaded photocatalysts prepared by IMP
$Rh_{2-x}Cr_xO_3$/18-STO(NCD)	cocatalyst-loaded photocatalysts prepared by NCD
Au	gold
$Au_{25}(SG)_{18}$	SG-protected Au_{25} clusters; Au_{25}/Cr_2O_3/18-STO(F-NCD) $Au_{25}(SG)_{18}$ was used as cocatalyst precursors, and the photocatalyst was prepared by the F-NCD method
Au_{25}/Cr_2O_3/18-STO(PD)	$Au_{25}(SG)_{18}$ was used as cocatalyst precursors, and the photocatalyst was prepared by the PD method
Au_{25}/Cr_2O_3/18-STO(NCD)	$Au_{25}(SG)_{18}$ was used as cocatalyst precursors, and the photocatalyst was prepared by the NCD method

■ REFERENCES

(1) Fujishima, A.; Honda, K. Electrochemical photolysis of water at a semiconductor electrode. *Nature* **1972**, *238*, 37−38.
(2) Wang, Q.; Domen, K. Particulate photocatalysts for light-driven water splitting: mechanisms, challenges, and design strategies. *Chem. Rev.* **2020**, *120*, 919−985.
(3) Kudo, A.; Miseki, Y. Heterogeneous photocatalyst materials for water splitting. *Chem. Soc. Rev.* **2009**, *38*, 253−278.
(4) Wang, Y.; Suzuki, H.; Xie, J.; Tomita, O.; Martin, D. J.; Higashi, M.; Kong, D.; Abe, R.; Tang, J. Mimicking natural photosynthesis: solar to renewable H_2 fuel synthesis by Z-scheme water splitting systems. *Chem. Rev.* **2018**, *118*, 5201−5241.
(5) Wang, Z.; Li, C.; Domen, K. Recent developments in heterogeneous photocatalysts for solar-driven overall water splitting. *Chem. Soc. Rev.* **2019**, *48*, 2109−2125.
(6) Pinaud, B. A.; Benck, J. D.; Seitz, L. C.; Forman, A. J.; Chen, Z.; Deutsch, T. G.; James, B. D.; Baum, K. N.; Baum, G. N.; Ardo, S.; Wang, H.; Miller, E.; Jaramillo, T. F. Technical and economic feasibility of centralized facilities for solar hydrogen production *via* photocatalysis and photoelectrochemistry. *Energy Environ. Sci.* **2013**, *6*, 1983−2002.
(7) Fabian, D. M.; Hu, S.; Singh, N.; Houle, F. A.; Hisatomi, T.; Domen, K.; Osterloh, F. E.; Ardo, S. Particle suspension reactors and materials for solar-driven water splitting. *Energy Environ. Sci.* **2015**, *8*, 2825−2850.
(8) Takata, T.; Jiang, J.; Sakata, Y.; Nakabayashi, M.; Shibata, N.; Nandal, V.; Seki, K.; Hisatomi, T.; Domen, K. Photocatalytic water splitting with a quantum efficiency of almost unity. *Nature* **2020**, *581*, 411−414.
(9) Kurashige, W.; Mori, Y.; Ozaki, S.; Kawachi, M.; Hossain, S.; Kawawaki, T.; Shearer, C. J.; Iwase, A.; Metha, G. F.; Yamazoe, S.; Kudo, A.; Negishi, Y. Activation of water-splitting photocatalysts by loading with ultrafine Rh−Cr mixed-oxide cocatalyst nanoparticles. *Angew. Chem., Int. Ed.* **2020**, *59*, 7076−7082.

(10) Kawawaki, T.; Mori, Y.; Wakamatsu, K.; Ozaki, S.; Kawachi, M.; Hossain, S.; Negishi, Y. Controlled colloidal metal nanoparticles and nanoclusters: recent applications as cocatalysts for improving photocatalytic water-splitting activity. *J. Mater. Chem. A* **2020**, *8*, 16081−16113.
(11) Kawawaki, T.; Kataoka, Y.; Ozaki, S.; Kawachi, M.; Hirata, M.; Negishi, Y. Creation of active water-splitting photocatalysts by controlling cocatalysts using atomically precise metal nanoclusters. *Chem. Commun.* **2021**, *57*, 417−440.
(12) Kraeutler, B.; Bard, A. J. Heterogeneous photocatalytic preparation of supported catalysts. Photodeposition of platinum on titanium dioxide powder and other substrates. *J. Am. Chem. Soc.* **1978**, *100*, 4317−4318.
(13) Zhang, G.; Lan, Z.-A.; Lin, L.; Lin, S.; Wang, X. Overall water splitting by Pt/g-C_3N_4 photocatalysts without using sacrificial agents. *Chem. Sci.* **2016**, *7*, 3062−3066.
(14) Martin, D. J.; Reardon, P. J. T.; Moniz, S. J. A.; Tang, J. Visible light-driven pure water splitting by a nature-inspired organic semiconductor-based system. *J. Am. Chem. Soc.* **2014**, *136*, 12568−12571.
(15) Domen, K.; Naito, S.; Soma, M.; Onishi, T.; Tamaru, K. Photocatalytic decomposition of water vapour on an NiO−$SrTiO_3$ catalyst. *J. Chem. Soc., Chem. Commun.* **1980**, 543−544.
(16) Shiraishi, Y.; Kofuji, Y.; Kanazawa, S.; Sakamoto, H.; Ichikawa, S.; Tanaka, S.; Hirai, T. Platinum nanoparticles strongly associated with graphitic carbon nitride as efficient co-catalysts for photocatalytic hydrogen evolution under visible light. *Chem. Commun.* **2014**, *50*, 15255−15258.
(17) Fina, F.; Ménard, H.; Irvine, J. T. S. The effect of Pt NPs crystallinity and distribution on the photocatalytic activity of Pt−g-C_3N_4. *Phys. Chem. Chem. Phys.* **2015**, *17*, 13929−13936.
(18) Jing, W.; Shen, H.; Qin, R.; Wu, Q.; Liu, K.; Zheng, N. Surface and interface coordination chemistry learned from model heterogeneous metal nanocatalysts: from atomically dispersed catalysts to atomically precise clusters. *Chem. Rev.* **2023**, *123*, 5948−6002.
(19) Kawawaki, T.; Kataoka, Y.; Hirata, M.; Iwamatsu, Y.; Hossain, S.; Negishi, Y. Toward the creation of high-performance heterogeneous catalysts by controlled ligand desorption from atomically precise metal nanoclusters. *Nanoscale Horiz.* **2021**, *6*, 409−448.
(20) Shi, Q.; Qin, Z.; Sharma, S.; Li, G. Recent progress in heterogeneous catalysis by atomically and structurally precise metal nanoclusters. *Chem. Rec.* **2021**, *21*, 879−892.
(21) Liu, X.; Wang, E.; Zhou, M.; Wan, Y.; Zhang, Y.; Liu, H.; Zhao, Y.; Li, J.; Gao, Y.; Zhu, Y. Asymmetrically doping a platinum atom into a Au_{38} nanocluster for changing the electron configuration and reactivity in electrocatalysis. *Angew. Chem., Int. Ed.* **2022**, *61*, No. e202207685.
(22) Kang, X.; Li, Y.; Zhu, M.; Jin, R. Atomically precise alloy nanoclusters: syntheses, structures, and properties. *Chem. Soc. Rev.* **2020**, *49*, 6443−6514.
(23) Chakraborty, I.; Pradeep, T. Atomically precise clusters of noble metals: emerging link between atoms and nanoparticles. *Chem. Rev.* **2017**, *117*, 8208−8271.
(24) Narouz, M. R.; Osten, K. M.; Unsworth, P. J.; Man, R. W. Y.; Salorinne, K.; Takano, S.; Tomihara, R.; Kaappa, S.; Malola, S.; Dinh, C.-T.; Padmos, J. D.; Ayoo, K.; Garrett, P. J.; Nambo, M.; Horton, J. H.; Sargent, E. H.; Häkkinen, H.; Tsukuda, T.; Crudden, C. M. N-heterocyclic carbene-functionalized magic-number gold nanoclusters. *Nat. Chem.* **2019**, *11*, 419−425.
(25) Pelicano, C. M.; Saruyama, M.; Takahata, R.; Sato, R.; Kitahama, Y.; Matsuzaki, H.; Yamada, T.; Hisatomi, T.; Domen, K.; Teranishi, T. Bimetallic synergy in ultrafine cocatalyst alloy nanoparticles for efficient photocatalytic water splitting. *Adv. Funct. Mater.* **2022**, *32*, 2202987.
(26) Negishi, Y.; Mizuno, M.; Hirayama, M.; Omatoi, M.; Takayama, T.; Iwase, A.; Kudo, A. Enhanced photocatalytic water splitting by $BaLa_4Ti_4O_{15}$ loaded with ∼1 nm gold nanoclusters using glutathione-protected Au_{25} clusters. *Nanoscale* **2013**, *5*, 7188−7192.
(27) Kurashige, W.; Kumazawa, R.; Ishii, D.; Hayashi, R.; Niihori, Y.; Hossain, S.; Nair, L. V.; Takayama, T.; Iwase, A.; Yamazoe, S.; Tsukuda, T.; Kudo, A.; Negishi, Y. Au_{25}-loaded $BaLa_4Ti_4O_{15}$ water-splitting photocatalyst with enhanced activity and durability produced using new chromium oxide shell formation method. *J. Phys. Chem. C* **2018**, *122*, 13669−13681.
(28) Tian, L.; Luo, Y.; Chu, K.; Wu, D.; Shi, J.; Liang, Z. A robust photocatalyst of Au_{25}@ZIF-8@TiO_2-ReP with dual photoreductive sites to promote photoelectron utilization in H_2O splitting to H_2 and CO_2 reduction to CO. *Chem. Commun.* **2019**, *55*, 12976−12979.
(29) Du, X. L.; Wang, X. L.; Li, Y. H.; Wang, Y. L.; Zhao, J. J.; Fang, L. J.; Zheng, L. R.; Tong, H.; Yang, H. G. Isolation of single Pt atoms in a silver cluster: forming highly efficient silver-based cocatalysts for photocatalytic hydrogen evolution. *Chem. Commun.* **2017**, *53*, 9402−9405.
(30) Mu, L.; Zhao, Y.; Li, A.; Wang, S.; Wang, Z.; Yang, J.; Wang, Y.; Liu, T.; Chen, R.; Zhu, J.; Fan, F.; Li, R.; Li, C. Enhancing charge separation on high symmetry $SrTiO_3$ exposed with anisotropic facets for photocatalytic water splitting. *Energy Environ. Sci.* **2016**, *9*, 2463−2469.
(31) Li, R.; Zhang, F.; Wang, D.; Yang, J.; Li, M.; Zhu, J.; Zhou, X.; Han, H.; Li, C. Spatial separation of photogenerated electrons and holes among {010} and {110} crystal facets of $BiVO_4$. *Nat. Commun.* **2013**, *4*, 1432.
(32) Kwak, K.; Choi, W.; Tang, Q.; Kim, M.; Lee, Y.; Jiang, D.-E.; Lee, D. A molecule-like $PtAu_{24}(SC_6H_{13})_{18}$ nanocluster as an electrocatalyst for hydrogen production. *Nat. Commun.* **2017**, *8*, 14723.
(33) Akinaga, Y.; Kawawaki, T.; Kameko, H.; Yamazaki, Y.; Yamazaki, K.; Nakayasu, Y.; Kato, K.; Tanaka, Y.; Hanindriyo, A. T.; Takagi, M.; Shimazaki, T.; Tachikawa, M.; Yamakata, A.; Negishi, Y. Metal single-atom cocatalyst on carbon nitride for the photocatalytic hydrogen evolution reaction: effects of metal species. *Adv. Funct. Mater.* **2023**, *33*, 2303321.
(34) Yazaki, D.; Kawawaki, T.; Hirayama, D.; Kawachi, M.; Kato, K.; Oguchi, S.; Yamaguchi, Y.; Kikkawa, S.; Ueki, Y.; Hossain, S.; Osborn, D. J.; Ozaki, F.; Tanaka, S.; Yoshinobu, J.; Metha, G. F.; Yamazoe, S.; Kudo, A.; Yamakata, A.; Negishi, Y. Carbon nitride loaded with an ultrafine, monodisperse, metallic platinum-cluster cocatalyst for the photocatalytic hydrogen-evolution reaction. *Small* **2023**, *19*, 2208287.
(35) Ohno, T.; Sarukawa, K.; Matsumura, M. Crystal faces of rutile and anatase TiO_2 particles and their roles in photocatalytic reactions. *New J. Chem.* **2002**, *26*, 1167−1170.
(36) Liu, G.; Yu, J. C.; Lu, G. Q.; Cheng, H.-M. Crystal facet engineering of semiconductor photocatalysts: motivations, advances and unique properties. *Chem. Commun.* **2011**, *47*, 6763−6783.
(37) Xie, Y. P.; Liu, G.; Yin, L.; Cheng, H.-M. Crystal facet-dependent photocatalytic oxidation and reduction reactivity of monoclinic WO_3 for solar energy conversion. *J. Mater. Chem.* **2012**, *22*, 6746−6751.
(38) Zhen, C.; Yu, J. C.; Liu, G.; Cheng, H.-M. Selective deposition of redox co-catalyst(s) to improve the photocatalytic activity of single-domain ferroelectric $PbTiO_3$ nanoplates. *Chem. Commun.* **2014**, *50*, 10416−10419.
(39) Dong, L.; Shi, H.; Cheng, K.; Wang, Q.; Weng, W.; Han, W. Shape-controlled growth of $SrTiO_3$ polyhedral submicro/nanocrystals. *Nano Res.* **2014**, *7*, 1311−1318.
(40) Maeda, K.; Teramura, K.; Masuda, H.; Takata, T.; Saito, N.; Inoue, Y.; Domen, K. Efficient overall water splitting under visible-light irradiation on $(Ga_{1-x}Zn_x)(N_{1-x}O_x)$ dispersed with Rh−Cr mixed-oxide nanoparticles: effect of reaction conditions on photocatalytic activity. *J. Phys. Chem. B* **2006**, *110*, 13107−13112.
(41) Maeda, K.; Domen, K. Photocatalytic water splitting: recent progress and future challenges. *J. Phys. Chem. Lett.* **2010**, *1*, 2655−2661.
(42) Pang, R.; Teramura, K.; Asakura, H.; Hosokawa, S.; Tanaka, T. Effect of thickness of chromium hydroxide layer on Ag cocatalyst surface for highly selective photocatalytic conversion of CO_2 by H_2O. *ACS Sustainable Chem. Eng.* **2019**, *7*, 2083−2090.

https://doi.org/10.1021/jacs.4c07351
J. Am. Chem. Soc. XXXX, XXX, XXX−XXX

(43) Su, S.; Siretanu, I.; van den Ende, D.; Mei, B.; Mul, G.; Mugele, F. Facet-dependent surface charge and hydration of semiconducting nanoparticles at variable pH. *Adv. Mater.* **2021**, *33*, 2106229.
(44) Walczak, M. M.; Popenoe, D. D.; Deinhammer, R. S.; Lamp, B. D.; Chung, C.; Porter, M. D. Reductive desorption of alkanethiolate monolayers at gold: a measure of surface coverage. *Langmuir* **1991**, *7*, 2687−2693.
(45) Alotabi, A. S.; Osborn, D. J.; Ozaki, S.; Kataoka, Y.; Negishi, Y.; Tesana, S.; Metha, G. F.; Andersson, G. G. Suppression of phosphine-protected Au_9 cluster agglomeration on $SrTiO_3$ particles using a chromium hydroxide layer. *Mater. Adv.* **2022**, *3*, 3620−3630.
(46) Kawawaki, T.; Kataoka, Y.; Hirata, M.; Akinaga, Y.; Takahata, R.; Wakamatsu, K.; Fujiki, Y.; Kataoka, M.; Kikkawa, S.; Alotabi, A. S.; Hossain, S.; Osborn, D. J.; Teranishi, T.; Andersson, G. G.; Metha, G. F.; Yamazoe, S.; Negishi, Y. Creation of high-performance heterogeneous photocatalysts by controlling ligand desorption and particle size of gold nanocluster. *Angew. Chem., Int. Ed.* **2021**, *60*, 21340−21350.
(47) Zutter, B.; Chen, Z.; Barrera, L.; Gaieck, W.; Lapp, A. S.; Watanabe, K.; Kudo, A.; Esposito, D. V.; Bala Chandran, R.; Ardo, S.; Talin, A. A. Single-particle measurements reveal the origin of low solar-to-hydrogen efficiency of Rh-doped $SrTiO_3$ photocatalysts. *ACS Nano* **2023**, *17*, 9405−9414.
(48) Miseki, Y.; Kato, H.; Kudo, A. Water splitting into H_2 and O_2 over niobate and titanate photocatalysts with (111) plane-type layered perovskite structure. *Energy Environ. Sci.* **2009**, *2*, 306−314.
(49) Konta, R.; Ishii, T.; Kato, H.; Kudo, A. Photocatalytic activities of noble metal ion doped $SrTiO_3$ under visible light irradiation. *J. Phys. Chem. B* **2004**, *108*, 8992−8995.
(50) Teitsworth, T. S.; Hill, D. J.; Litvin, S. R.; Ritchie, E. T.; Park, J.-S.; Custer, J. P., Jr.; Taggart, A. D.; Bottum, S. R.; Morley, S. E.; Kim, S.; McBride, J. R.; Atkin, J. M.; Cahoon, J. F. Water splitting with silicon p−i−n superlattices suspended in solution. *Nature* **2023**, *614*, 270−274.
(51) Zhou, P.; Navid, I. A.; Ma, Y.; Xiao, Y.; Wang, P.; Ye, Z.; Zhou, B.; Sun, K.; Mi, Z. Solar-to-hydrogen efficiency of more than 9% in photocatalytic water splitting. *Nature* **2023**, *613*, 66−70.

https://doi.org/10.1021/jacs.4c07351
J. Am. Chem. Soc. XXXX, XXX, XXX−XXX